Chemical Physics Letters 658 (2016) 248–253

Contents lists available at ScienceDirect

Chemical Physics Letters

journal homepage: www.elsevier.com/locate/cplett

Research paper

Influence of cation substitution on the crystal structure and luminescent properties in apatite structural $Ba_{4.97-x}Sr_x(PO_4)_3Cl{:}0.03Eu^{2+}$ phosphors

Ling Zhu [a], Zhaohui Huang [a,*], Maxim S. Molokeev [b,c], Xin Min [a], Yangai Liu [a], Minghao Fang [a], Xiaowen Wu [a]

[a] School of Materials Science and Technology, National Laboratory of Mineral Materials, China University of Geosciences, Beijing 100083, China
[b] Laboratory of Crystal Physics, Kirensky Institute of Physics, SB RAS, Krasnoyarsk 660036, Russia
[c] Department of Physics, Far Eastern State Transport University, Khabarovsk 680021, Russia

ARTICLE INFO

Article history:
Received 15 April 2016
In final form 22 June 2016
Available online 22 June 2016

Keywords:
Substitution
Apatite
$Ba_{4.97-x}Sr_x(PO_4)_3Cl{:}0.03Eu^{2+}$
Luminescence

ABSTRACT

A series of apatite-type phosphors $Ba_{4.97-x}Sr_x(PO_4)_3Cl{:}Eu^{2+}$($x$ = 0, 0.5, 1.0, 1.5, 2.0) were synthesized by the high temperature solid-state reaction method, and its luminescence properties were investigated in detail. It can be found that a red shift of the emission peak wavelength emerged from 439 to 462 nm with the continuous introduction of Sr^{2+} into the crystal lattice which has been simulated by a crystal-field model. The red shift is explained by the distortion in the crystal structure through X-ray diffraction and the Rietveld refinement analysis. According to a recently raised structural model, Eu^{2+} ions are surrounded by O atoms, PO_4 tetrahedrons and Ba/Sr ions. After introducing Sr^{2+} into the lattice, the interatomic distance between Ba/Sr atoms and Eu^{2+} was expected to become shorter, resulting in a distortion of the inner EuO_n polyhedrons. Then the crystal field strength surrounding Eu^{2+} was increased, finally resulting in the red shift.

1. Introduction

Eu^{2+} is an important activator ion among the rare earth ions, widely used in UV or blue light excitated phosphor. Generally, Eu^{2+} emission results from f-f transition and d-f transition [1]. The most common is due to the $4f^6 5d$-$4f^7$ transitions between energy levels [2]. However, the transition $4f \rightarrow 4f5d$ is very sensitive to the crystal field environment, resulting in the broad emissions band from blue to red regions in different host matrix [3–6]. While Eu^{2+} can emit light from the ultraviolet to the infrared broadband emitting fluorescence in different matrixes due to the impact of the strength of the crystal field and covalent. As a result, the exploration of a single-composition color-tunable phosphor using the cation substitution on the structure and photoluminescence properties become a hot issue. As we known, the apatite compound is a kind of useful phosphor hosts and has been widely studied as matrix lattice for luminescence materials. Therefore, the study on the apatite compound is of significance and valuable, as they possess the capability of substituting by versatile ions and forming solid solution.

Apatite, with a general formula of $A_5(BO_4)_3C$, has a hexagonal structure and belongs to the space group $P6_3/m$, wherein, A is a mono-, di or tri-divalent cation such as K^+, Na^+, Mn^{2+}, Ca^{2+}, Sr^{2+}, Ba^{2+} or Ce^{3+}, BO_4 represents an anion group including SO_4^{2-}, PO_4^{3-}, VO_4^{3-}, SiO_4^{4-}, and C is occupied by anion F^-, Cl^-, Br^-, O^- or OH^- [7–9]. In the structure of $Ba_5(PO_4)_3Cl$, the Ba atoms are arranged on two non-equivalent sites, Ba(1) and Ba(2). Ba(1) ions at site one are coordinated by nine oxygen atoms while Ba(2) ions at site two are surrounded by six oxygen atoms plus two chlorine atoms [10]. The luminescence property of the phosphor is greatly influenced by the presence of two non-equivalent sites [11]. Apatite-type compound have been extensively used as a host lattice for luminescent ions, and confirmed as an efficient luminescent material for display and white light emitting diodes (WLEDs) applications. In the recent years, apatite structural phosphors doped with rare earth ions have been reported in the literature [12–16].

In the $Ba_5(PO_4)_3Cl{:}Eu^{2+}$ matrix, the location of cation is substituted by Eu^{2+} ions. Hence, the introduction of new ions (such as Sr ion) into Ba(1) and Ba(2), would have a direct effect on the crystalline field around the luminescent center (Eu^{2+} ions) which affect the luminescence properties further. Deressa et al. reported blue-emitting apatite-type structural $(Sr,Ba)_5(PO_4)_3Cl{:}Eu^{2+}$ phosphors for application in near-UV pumped white LED and studied the luminescence and thermal quenching properties of

* Corresponding author.
E-mail address: huang118@cugb.edu.cn (Z. Huang).

http://dx.doi.org/10.1016/j.cplett.2016.06.061
0009-2614/

$(Sr,Ba)_5(PO_4)_3Cl:Eu^{2+}$ phosphor [17]. However, the mechanism of emission wavelength tunable phenomenon is not clear at present. Hence, according to recent raised structure model discussing the relationship between luminescence properties and distortion of crystal structure [18,19], we look forward to providing one way to explain the luminescence mechanism and solve relevant problems in the present phosphor case.

2. Experimental

2.1. Materials and preparation

$Ba_{4.97-x}Sr_x(PO_4)_3Cl:0.03Eu^{2+}$($x$ = 0, 0.5, 1.0, 1.5, 2.0) were synthesized by the high temperature solid-state reaction using $BaCO_3$, $BaCl_2{\cdot}2H_2O$, $SrCO_3$, $SrCl_2{\cdot}6H_2O$, $NH_4H_2PO_4$ and Eu_2O_3 as raw materials. The purity of $BaCO_3$, $SrCO_3$ and $NH_4H_2PO_4$ is A.R., and that of Eu_2O_3 is 99.99%. Stoichiometric amounts of the staring reagents were thoroughly mixed and ground together, and excess $BaCl_2{\cdot}2H_2O$ and $SrCl_2{\cdot}6H_2O$ were added as an annexing agent in case of volatilization at high temperature. The mixture was preheated at 500 °C for 2 h in the air, and cooled down slowly to room temperature. Then the sample was reground in an agate mortar for 15 min and reheated at 1200 °C for 4 h in a 90%N_2–10%H_2 atmosphere and was allowed to cool in the reducing atmosphere to room temperature. Finally, the obtained products were ground into powder for measuring phase compositions and photoluminescence properties.

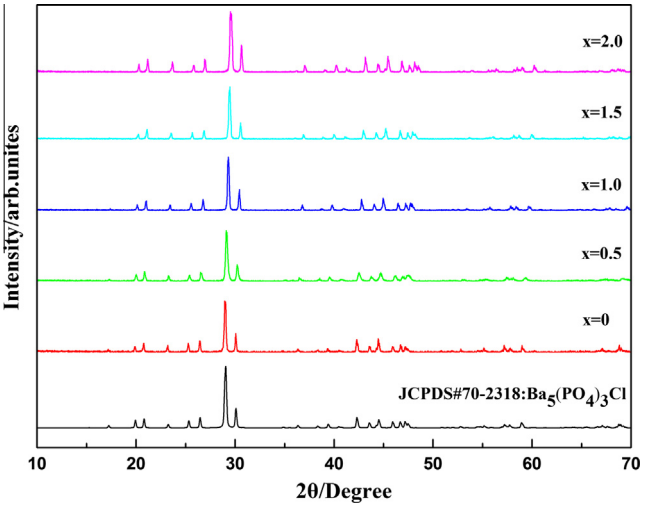

Fig. 1. XRD patterns of the $Ba_{4.97-x}Sr_x(PO_4)_3Cl:0.03Eu^{2+}$ phosphors.

2.2. Characterization

The phase compositions were determined by X-ray diffraction (XRD; D8 Advance diffractometer, Germany). The powder diffraction patterns of $Ba_{4.97-x}Sr_x(PO_4)_3Cl:Eu^{2+}$ phosphors for Rietveld analysis were collected with a step size of 0.02° and a step scanning rate of 2 s/step and the Rietveld refinement was performed by using TOPAS 4.2. The photoluminescence excitation (PLE) and emission (PL) spectra were recorded using a HITACH F-4500 fluorescence spectrophotometer at room temperature with a photomultiplier tube operating at 400 V and a 150 W Xe lamp used as the excitation lamp.

3. Results and discussion

3.1. XRD patterns and crystal structure refinement of $Ba_{4.97-x}Sr_x(PO_4)_3Cl:0.03Eu^{2+}$

XRD patterns of $Ba_{4.97-x}Sr_x(PO_4)_3Cl:0.03Eu^{2+}$ (x = 0, 0.5, 1.0, 1.5, 2.0) were shown in Fig. 1. All the peaks matches well with the standard XRD pattern of $Ba_5(PO_4)_3Cl$ (JCPDS No. 70-2318) except for a slight peak shift due to expected decrease of cell parameters, and no other impurity phases were detected. This indicate that Eu^{2+} and Sr^{2+} ions were completely doped in the host lattices during the synthesis process.

The selected samples $Ba_{4.47}Sr_{0.5}(PO_4)_3Cl:0.03Eu^{2+}$ (x = 0.5) and $Ba_{3.97}Sr(PO_4)_3Cl:0.03Eu^{2+}$ (x = 1.0) were then refined using the Rietveld method. The single crystal structure data of $Ba_5(PO_4)_3Cl$ (ICSD No. 8191; apatite type structure) was used as a starting model to refine the crystal structure. The observed (red), calculated (black) and difference (grey) XRD profiles for the refinement are shown in Fig. 2. The structure refinement was stable and ended with low R-factors as shown in Table 1. The lattice parameters determined from whole profile Rietveld refinement are listed in Table 1. The samples (x = 0, 0.5, 1.0) with hexagonal structure (space group $P6_3/m$) are coincident with the apatite-type $Ba_5(PO_4)_3Cl$ [20], indicating that the doping ions were well resolved into host lattices with no significant change in the crystal structure.

From Table 1, it can be also seen that the unit cell volume decreased with the increase of x value. The radii of Ba^{2+}, Sr^{2+} and Eu^{2+} ions with different coordination number are shown in Table 2, which shows that the radii of Sr^{2+} and Eu^{2+} are smaller than that of Ba^{2+}. When larger Ba^{2+} are replaced by the smaller Sr^{2+} and Eu^{2+} ions, the cell lattice would reduce, resulting in the decrease of unit cell volume with increasing Sr^{2+} concentration. These results also indicate the substitution of Ba^{2+} by Eu^{2+} and Sr^{2+} ions and further confirmed that $Ba_{4.47}Sr_{0.5}(PO_4)_3Cl:0.03Eu^{2+}$ samples are pure phase forming solid solution.

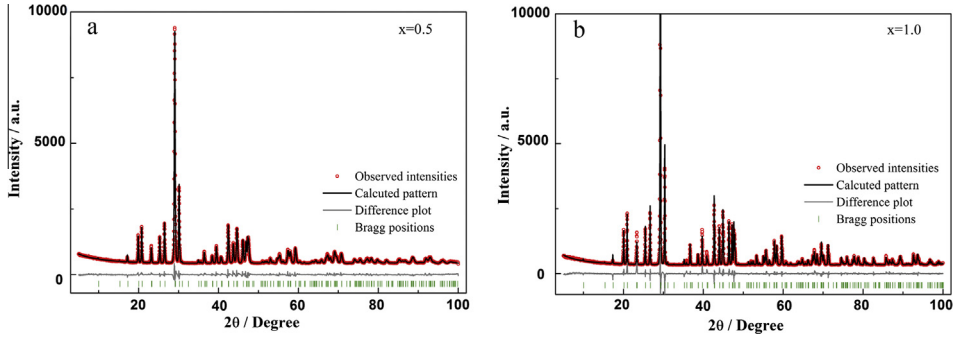

Fig. 2. Observed (red), calculated (black), and difference (gray) XRD profiles for the refinement of samples $Ba_{4.47}Sr_{0.5}(PO_4)_3Cl:0.03Eu^{2+}$ (x = 0.5) and $Ba_{3.97}Sr(PO_4)_3Cl:0.03Eu^{2+}$ (x = 1.0) by Rietveld method. Bragg reflections are indicated with tick marks. (For interpretation of the references to color in this figure legend, the reader is referred to the web version of this article.)

Table 1
Crystallographic data and details in the data collection and refinement parameters for the $Ba_{4.97-x}Sr_x(PO_4)_3Cl:0.03Eu^{2+}$ ($x = 0$, 0.5, 1.0) Samples.

	$Ba_{4.97}(PO_4)_3Cl$	$Ba_{4.47}Sr_{0.5}(PO_4)_3Cl$	$Ba_{3.97}Sr(PO_4)_3Cl$
x	0	0.5	1
Space group	$P6_3/m$	$P6_3/m$	$P6_3/m$
a, Å	10.2689 (1)	10.2211 (4)	10.1660 (1)
c, Å	7.6499 (1)	7.6193 (3)	7.5809 (1)
V, Å^3	698.61 (2)	689.35 (7)	678.50 (2)
2θ interval, deg	5–100	5–100	5–100
No. of reflections	268	263	261
No. of refined parameters	37	37	37
R_{wp}, %	13.511	11.772	13.340
R_p, %	9.961	7.910	9.827
R_{exp}, %	7.914	7.404	7.260
χ^2	2.914	2.528	3.375
R_B, %	6.702	3.004	6.307

Table 2
Comparison of effective ionic radii of Ba^{2+}, $Sr^{2+}$and Eu^{2+} in both crystallographic sites.

Site	CN	Effective ionic radii (Å)		
		Ba^{2+}	Sr^{2+}	Eu^{2+}
Ba1/Sr1/Eu1	9	1.47	1.31	1.30
Ba2/Sr2/Eu2	8	1.42	1.26	1.25

3.2. Photoluminescence properties of the $Ba_{4.97-x}Sr_x(PO_4)_3Cl:0.03Eu^{2+}$ phosphors

The primitive part of the $Ba_5(PO_4)_3Cl$ unit cell has two Ba sites, Ba(1) with C_3 point symmetry is surrounded by nine oxygen anions while the other site Ba(2) with C_s point symmetry is surrounded by six oxygen anions plus two Cl anion [21]. The Sr/Eu ions could be located in both of these sites. The crystal structure of the sample $Ba_{3.97}Sr(PO_4)_3Cl:0.03Eu^{2+}$ ($x = 1$) is shown in Fig. 3, which also presents the Ba1/Sr1/Eu1 position coordinated with nine oxygen atoms and Ba2/Sr2/Eu2 coordinated with six oxygen atoms plus two chlorine atoms, respectively. In addition, the replacement of Ba by Sr does not change the space group.

The photoluminescence (PL) excitation and emission spectra of the $Ba_{4.97-x}Sr_x(PO_4)_3Cl:0.03Eu^{2+}$ ($0 \leqslant x \leqslant 2$) phosphors with respect to the cation substitution was characterized. As shown in Fig. 4(a), all samples can be excited in near ultraviolet region, and the excitation efficiency of samples were high especially in the range from 250 nm to 400 nm. It also can be seen from Fig. 4 (b) that the sample $Ba_{4.97}(PO_4)_3Cl:0.03Eu^{2+}$ ($x = 0$) emits blue light with a relatively narrow symmetric band centered at 439 nm. This emission can be decomposed into two well-separated Gaussian components correspond to the two cation sites in the crystal lattice with maxima at 437 nm and 460 nm as shown in Fig. 5a. The position of the d-band edge (E) in energy for the rare earth ions can be calculated as follow [22]

$$E = Q\left[1 - \left[V/4^{1/v}10^{-n^* ea^* r/80}\right]\right] \quad (1)$$

where Q is the position in energy for the lower d-band edge of the free ion, generally 34,000 cm^{-1} for Eu^{2+}; V is the valence of the active cation, $V = 2$ for Eu^{2+}; n is the number of anions in the immediate shell about the ion, 9 and 8 for EuO_9 and EuO_8, respectively; ea is the electron affinity of the atoms (for most oxides $ea = 1.6$) that form the anions and r is the radius of the host cation replaced by the active cation, Eu^{2+} in this case. The effective ionic radii of Ba^{2+} are $r = 1.42$ Å for CN = 8 and $r = 1.47$ Å for CN = 9. It was calculated that $E = 20{,}927$ cm^{-1} and $E = 19{,}752$ cm^{-1} for Eu in Ba(1) and Ba (2) sites, respectively. E is a parameter related to wavelength (λ), using the following empirical equation [23]

$$E\lambda = hc \quad (2)$$

where h is the Plank constant (6.63×10^{-34} J × s) and c is the value of velocity of light (3×10^8 m/s). We can calculated that $\lambda = 478$ nm and 506 nm for Eu in Ba(1) and Ba(2) sites, respectively. It can be seen that the calculated values of $\lambda = 478$ nm for Eu in Ba1 is close to the observed value of $\lambda = 437$ nm. Similarly, the calculated value

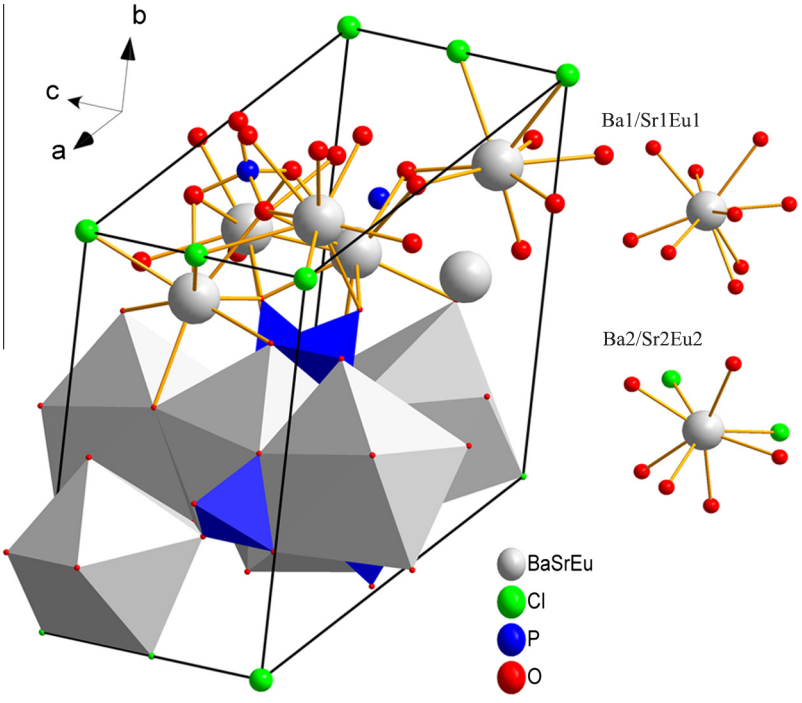

Fig. 3. Crystal structure of the sample $Ba_{3.97}Sr(PO_4)_3Cl:0.03Eu^{2+}$ ($x = 1$) and coordination of the cation ions with oxygen atoms.

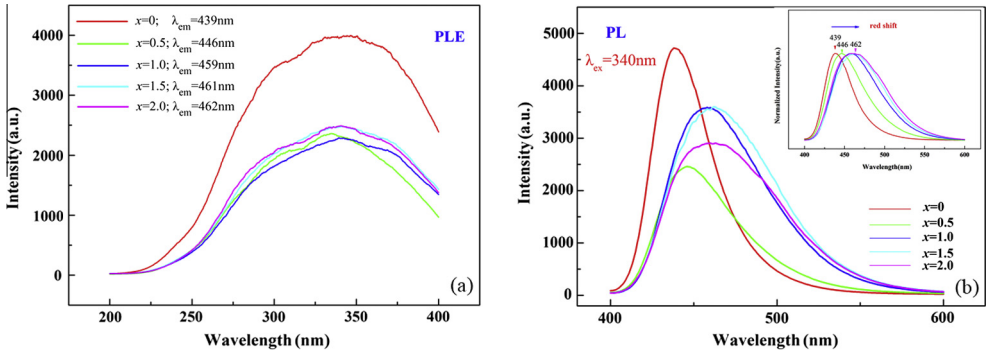

Fig. 4. Photoluminescence excitation(a) and emission(b) spectra of $Ba_{4.97-x}Sr_x(PO_4)_3Cl:Eu^{2+}$ ($x = 0–2$) obtained at room temperature using the maximum emission wavelength for each sample. The inset of (b) shows the normalized photoluminescence emission spectra.

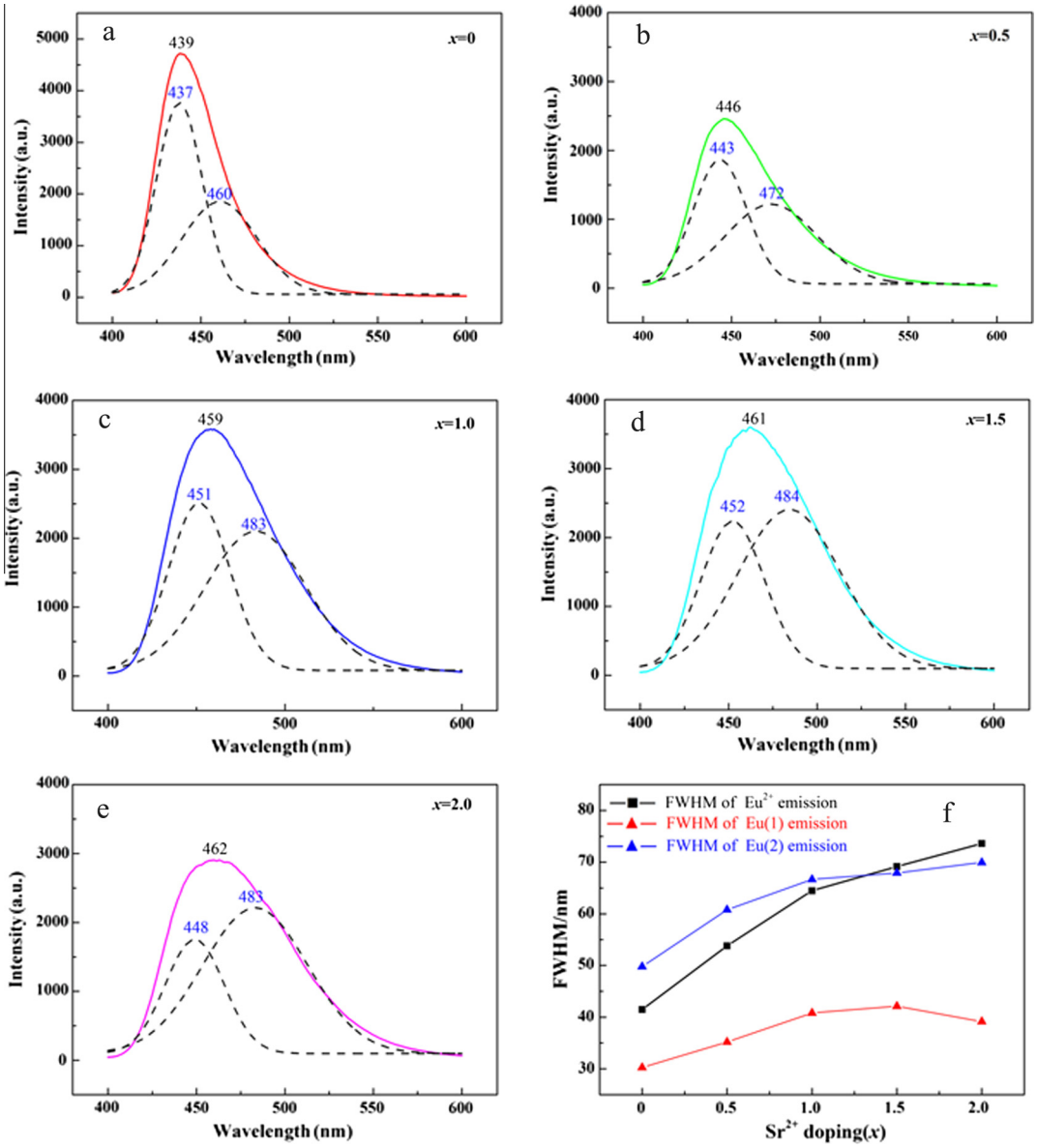

Fig. 5. Emission spectra fit to two Gaussian functions for $x = 0$, $x = 0.5$, $x = 1.0$, $x = 1.5$ and $x = 2.0$ show the contribution to the emission spectra from Eu^{2+} in two distinct crystallographic sites. Dashed lines represent the individual Gaussian functions. The FWHM of the Eu^{2+}, Eu (1) site and Eu (2) site emission in $Ba_{4.97-x}Sr_x(PO_4)_3Cl:0.03Eu^{2+}$ ($x = 0–2$) were presented in inset f.

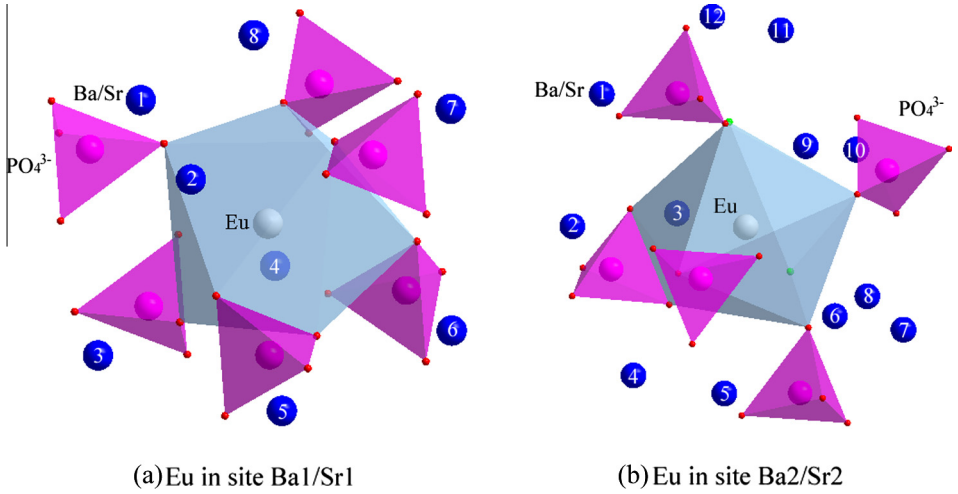

Fig. 6. First three nearest coordination sphere of Eu ions which are determined to be located in the two Sr/Ba site in the unit cell of $Ba_{4.97-x}Sr_x(PO_4)_3Cl:Eu^{2+}$. The first, second, and third coordination spheres of Eu^{2+} consist of O atoms, PO_4 tetrahedrons and Sr/Ba ions, respectively. Eu(1) site has eight coordinating Ba/Sr ions while Eu(2) has twelve coordinating Ba/Sr ions which are marked by numbers, respectively.

of $\lambda = 506$ nm is close to the observed value of $\lambda = 460$ nm for Eu in Ba(2) site. Therefore, we propose that the emission peak centered at 437 and 460 nm are attributed to Eu^{2+} ions occupying the Ba(1) site with nine-coordination and Ba(2) site with eight-coordination, respectively.

In case of Sr doping into $Ba_{4.97}(PO_4)_3Cl:0.03Eu^{2+}$, the samples exhibit a broad asymmetric band emission with a red shift of the emission peak from 439 to 462 nm, as shown in Fig. 4(b).

The emission band of two site in the samples ($x = 0$, 0.5, 1.0, 1.5, 2.0) were obtained by Gaussian deconvolution (Fig. 5(a)–(e). With the increase of Sr^{2+} concentration, the emission wavelength of site (1) exhibits red shift from 437 nm to 452 nm. The red shift was also observed in site(2) from 460 nm to 484 nm. However, the red shift was inhibited when $x = 2$. The samples with $x > 2$ synthesized by the same method also shows that the maximum red shift happened at $x = 2$. The FWHM (full width at half maximum) values of PL spectra enhanced with the increase in x from 0 to 2 as shown in Fig. 5f, resulting in the broad asymmetric emission band.

The phenomenon of the red shift can be explained from the aspect of crystal structure. The coordination spheres around Eu^{2+} sites are shown in Fig. 6 according to a recently raised structural model [16]. As can be seen, the first, second, and third coordination spheres of Eu^{2+} ions consist of O atoms, PO_4 tetrahedrons, and Ba/Sr ions, respectively. At the two sites, different forms of EuO_n polyhedrons and different numbers of coordinating PO_4 tetrahedrons and neighboring Ba/Sr ions are observed.

In $Ba_3(PO_4)_3Cl:Eu^{2+}$ structure, the Eu(1) site are coordinated by eight nearby Ba ions in the third coordination sphere and form the EuO_n–Ba_8 blocks, while Eu(2) site are coordinated by twelve nearby Ba ions in the third coordination sphere and form the EuO_n–Ba_{12} blocks, which emits blue light under UV excitation. On doping with Sr ions, in addition to the EuO_n–Ba_8 and EuO_n–Ba_{12} blocks, EuO_n–$Ba_{8-x}Sr_x$ ($x = 1, 2, \ldots, 7, 8$) and EuO_n–$Ba_{12-y}Sr_y$ ($y = 1, 2, \ldots, 11,12$) blocks appeared. Due to the increase in doping concentration of smaller Sr^{2+} ions, the interatomic distance between the third coordination sphere (Ba/Sr) and the first coordination sphere (Eu^{2+}) was expected to become shorter, resulting in enhanced interaction [24]. Then the incorporation of smaller Sr^{2+} ions into the structure increased the internal pressure on the lattice and leads to a distortion of the inner EuO_n polyhedrons. The crystal field strength surrounding Eu^{2+} was thus increased, finally resulting in tunable PL properties.

4. Conclusions

Cation substitution dependent tunable broad asymmetric photoluminescence behavior was observed in $Ba_{4.97-x}Sr_x(PO_4)_3Cl:0.03Eu^{2+}$ ($0 \leqslant x \leqslant 2$) phosphors. The Rietveld refinements verified the phase purity and apatite type crystal structure of the phosphors. With doping Sr^{2+} ions into the crystal lattice, the different value of PL emission wavelength of two cation sites increase resulting in a broader spectrum. The tunable photoluminescence evolution was also studied as a function of Sr concentration, over the composition range $0 \leqslant x \leqslant 2$. In addition to the emission band peak at 439 nm in $Ba_{4.97}(PO_4)_3Cl:0.03Eu^{2+}$ ($x = 0$), the substitution of Ba^{2+} by Sr^{2+} induced the emerging broad-band peak at 439–462 nm. A red shift of the emission peak located in the blue region is observed on an increase of x in the samples with $0 \leqslant x \leqslant 2$. This phenomenon could be related to the EuO_n–Ba and EuO_n–Ba/Sr emitting blocks, respectively.

Acknowledgment

This present work was supported by the National Natural Science Foundations of China (Grant Nos. 51472222 and 51372232), the Fundamental Research Funds for the Central Universities (Grant No. 2652015310), and the Research Fund for the Doctoral Program of Higher Education of China (Grant No. 20130022110006).

References

[1] C. Wang, The Department of Physics in Peking University, 2011.
[2] Q.F. Guo, L.B. Liao, L.F. Mei, H.K. Liu, J. Solid State Chem. 226 (2015) 107.
[3] P.S. Thakre, S.C. Gedam, S.J. Dhoble, R.G. Atram, J. Lumin. 131 (2011) 2683.
[4] J.J. Yu, W.T. Gong, Z.G. Xiao, G.L. Ning, J. Lumin. 132 (2012) 2957.
[5] Z.G. Xia, Q. Li, J.Y. Sun, Mater. Lett. 61 (2007) 1885.
[6] Z.G. Xia, X.M. Wang, Y.X. Wang, L.B. Liao, X.P. Jing, Inorg. Chem. 50 (2011) 10134.
[7] Y.C. Li, Y.H. Chang, B.S. Tsai, Y.C. Chen, Y.F. Lin, J. Alloys Compd. 416 (2006) 199.
[8] N. Lakshminarasimhan, U.V. Varadaraju, J. Solid State Chem. 178 (2005) 3284.
[9] Y.Q. Shen, R. Chen, F. Xiao, H.D. Sun, A. Tok, Z.L. Dong, J. Solid State Chem. 183 (2010) 3093.
[10] C.X. Li, Y.H. Duan, W.C. Hu, J. Alloys Compd. 619 (2015) 66.
[11] I.M. Nagpure, S.S. Pitale, E. Coetsee, O.M. Ntwaeaborwa, J.J. Terblans, H.C. Swart, Phys. B: Condens. Matter 407 (2012) 1505.
[12] J.H. Zhang, H.B. Liang, R.J. Yu, H.B. Yuan, Q. Su, Mater. Chem. Phys. 114 (2009) 242.

[13] Y.H. Song, H.P. You, M. Yang, Y.H. Zheng, K. Liu, G. Jia, Y.J. Huang, L.H. Zhang, H. J. Zhang, Inorg. Chem. 49 (2010) 1674.
[14] J. Yu, C.F. Guo, Z.Y. Ren, J.T. Bai, Opt. Laser Technol. 43 (2011) 762.
[15] H.B. Liang, Q. Zeng, Z.F. Tian, H.H. Lin, Q. Su, G.B. Zhang, Y.B. Zhang, Cheminform 154 (2007) 177.
[16] Q. Zeng, H.B. Liang, G.B. Zhang, M.D. Birowosuto, Z.F. Tian, H.H. Lin, Y.B. Fu, P. Dorenbos, Q. Su, J. Phys. Condens. Matter 18 (2006) 9549.
[17] G. Deressa, K.W. Park, H.S. Jeong, S.G. Lim, H.J. Lim, Y.S. Jeong, J.S. Kim, J. Lumin. 161 (2015) 347.
[18] H.P. Ji, Z.H. Huang, Z.G. Xia, M.S. Molokeev, V.V. Atuchin, S.F. Huang, Inorg. Chem. 53 (2014) 11119.
[19] H.P. Ji, Z.H. Huang, Z.G. Xia, M.S. Molokeev, V.V. Atuchin, M.H. Fang, S.F. Huang, Inorg. Chem. 53 (2014) 5129.
[20] M. Hata, F. Marumo, S. Iwai, H. Aoki, Acta Crystallogr. 35 (2007) 2382.
[21] M.B. Xie, R.K. Pan, Opt. Mater. 35 (2013) 1162.
[22] L.G. Van Uitert, J. Lumin. 29 (1984) 1.
[23] Q. Fei, C.K. Chang, D. Mao, J. Alloys Compd. 390 (2005) 133.
[24] Z.G. Xia, H.Y. Du, J.Y. Sun, D.M. Chen, X.F. Wang, Mater. Chem. Phys. 119 (2010) 7.